Enhancing final image contrast in off-axis digital holography using residual fringes

MANUEL BEDROSSIAN[1], J. KENT WALLACE[2], EUGENE SERABYN[2], CHRISTIAN LINDENSMITH[2], AND JAY NADEAU[3]

[1]*Department of Medical Engineering, California Institute of Technology. 1200 E. California Blvd. Pasadena CA 91125*
[2]*Jet Propulsion Laboratory, California Institute of Technology. 4800 Oak Grove Dr. Pasadena CA 91011*
[3]*Department of Physics, Portland State University. Portland OR 97201*
**nadeau@pdx.edu*

Abstract: We show that background fringe-pattern subtraction is a useful technique for removing static noise from off-axis holographic reconstructions and can enhance image contrast in volumetric reconstructions by an order of magnitude. We demonstrate the fundamental principle of this technique and introduce some practical considerations that must be made when implementing this scheme. This work also shows an experimental verification of the background fringe subtraction scheme using various biological samples.

1. Introduction

Digital off-axis holography is an imaging technique that is capable of capturing both the amplitude and phase of light using a single intensity image (hologram) [1]. It suffers from various types of noise, however, which include but are not limited to photon (shot and speckle) noise, and detector noise (dark noise, read noise, and quantization noise) [2]. Removal of the zero-order and twin-image terms is straightforward in off-axis holography [3], and much effort has been devoted to reducing residual noise in holographic reconstructions due to phase aberrations [4], astigmatism, spherical aberrations, and anamorphism [5-7]. However, one problem with off-axis holography is slight temporal variations, which make the extended background fringe and speckle pattern difficult to remove to deep levels without the use of computationally expensive methods.

Here we present a computationally inexpensive method of removing the dominant static noise terms from off-axis holographic images. This method involves the background subtraction of raw holograms prior to numerical reconstruction. By only reconstructing the residual localized fringe packets remaining after subtraction of the background fringe pattern, noise contributions such as speckle are removed prior to propagation through the reconstruction process. A theoretical explanation of the approach is presented, as well as practical considerations when implementing this technique. Finally, processing of experimental data from cultures of bacterial and protozoa cells near the resolution limit of the instrument is shown, highlighting this technique's utility.

2. Principle of Operation

Figure 1A and 1B show the optical schematic and laboratory image of a common path DHM instrument described in [8-10], which was used for the experimental data presented in this work. A coherent light source is collimated and passed through two identically sized microfluidic wells. One contains the object of interest while the other contains a reference liquid in order to match optical path lengths with the sample well. The sample and reference beams are then

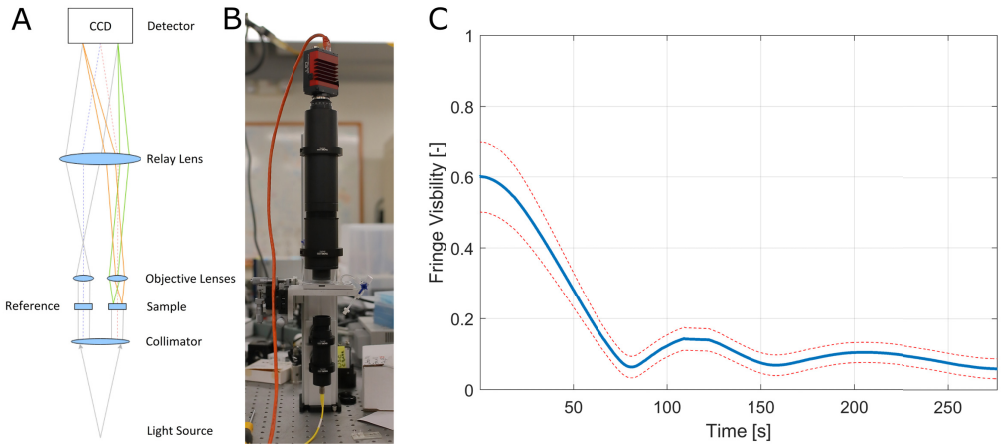

Fig. 1. Optical Schematic of the DHM instrument used throughout this work (A), an image of the benchtop instrument (B), and fringe stability of the DHM instrument as a function of time (C). Centerline indicates the mean fringe visibility and dashed lines indicate the 95% confidence interval range.

Table 1. Properties of the common path DHM instrument

Property	**Value [unit]**
Operating wavelengths	405 [nm]
	520 [nm]
	625 [nm]
Numerical aperture	0.38 [-]
System magnification	19.7 [-]
Lateral resolution	0.7 [μm]

passed through two separate but identical objective lenses. Finally, a relay lens recombines the beams at a detector plane, creating an interferogram (hologram).

Let two monochromatic and coherent beams, $O(x,y,t)$ and $R(x,y)$, corresponding to the object and reference beam, respectively, be incident on an optical detector, such that the resulting interference pattern recorded by the digital detector is

$$I(x,y,t) = (O+R)(O+R)^* = |O|^2 + |R|^2 + RO^* + R^*O, \quad (1)$$

where x, y are spatial coordinates within the hologram, and t is time. The object beam can be expressed as the superposition of a static beam $O_S(x,y)$ and spatiotemporal deviations from that static beam $\epsilon(x,y,t)$, such that $O = O_s + \epsilon$. Thus, the hologram can be expressed as

$$I(x,y,t) = |O_s|^2 + |\epsilon|^2 + |R|^2 + RO_s^* + R^*O_s + (O_S + R)\epsilon^* + (O_S + R)^*\epsilon. \quad (2)$$

The temporally averaged hologram is defined as

$$\bar{I}(x,y) = |O_s|^2 + \overline{|\epsilon|^2} + |R|^2 + RO_s^* + R^*O_s + (O_S + R)\bar{\epsilon}^* + (O_S + R)^*\bar{\epsilon}. \quad (3)$$

For a sufficiently large timescale, it can be assumed that $\bar{\epsilon} = 0$. The residual hologram is defined as the difference between Equations 2 and 3:

$$I_R(x,y,t) = I(x,y,t) - \bar{I}(x,y) = O_S\epsilon^* + O_S^*\epsilon + R\epsilon^* + R^*\epsilon + |\epsilon|^2 - \overline{|\epsilon|^2}. \quad (4)$$

The O_S and ϵ beams are on-axis with each other and thus their interference terms only contribute to the zero-order term of Equations 3 and 4. The term $|\epsilon|^2 - \overline{|\epsilon|^2}$ is also a zero-order term. Using typical techniques of Fourier-space spatial filtering, which removes zero-

order and twin image artifacts from the reconstructed images [3], the spatially filtered hologram that becomes reconstructed can be expressed as $I_R^F = R^* \epsilon$.

3. Practical Considerations

Background subtraction of holograms is useful because any stationary artifacts in the image become attenuated, leaving only dynamic objects. If the background fringes of the hologram are stable, these fringes would be effectively removed from the resulting image, except for localized fringe 'packets' associated with any particle that has moved through the field of view of the hologram. This background subtraction technique vastly increases the signal to noise ratio of any dynamic particle in an image sequence, making it much easier for automated particle detection algorithm to detect particles of interest in space and time. We show here that rapid motion is not necessary for the method to work; movement as small as bacterial Brownian motion will suffice.

Such a background subtraction technique requires a stable interferometer. Many sources of noise can introduce shifts in DHM fringes, causing them to drift across the field of view of the detector. These noise sources include but are not limited to speckle noise, temporal phase noise caused by uncorrelated variations between the two beams of the instrument, as well as changes in illumination wavelength from instabilities in the illumination source. These sources of noise introduce an upper limit on the timescales where the proposed background subtraction scheme is useful. As the background fringes shift, they will by definition become dynamic objects in the image, thus no longer being removed by the background subtraction scheme.

The data used here was taken with a common-path off-axis DHM described previously [8], with parameters in Table 1. The valid timescales of this background subtraction technique were quantified by collecting holographic images as a function of time without a sample in the field of view of the instrument. Temporally averaged holograms were calculated at various timescales through the hologram sequence. Fringe stability was inferred by calculating the average fringe visibility of the temporally averaged hologram. This is possible because if the fringes are absolutely stable (static), the temporally averaged hologram would equal the fringe pattern of each hologram in the sequence. As the fringe pattern begins to shift, they will by definition become dynamic artifacts in the image and thus not appear in the temporally averaged hologram. Figure 1C shows a plot of fringe stability as a function of time for the DHM instrument used throughout this work. The center line in the plot signifies the mean fringe visibility value while the dotted lines signify the 95% confidence interval value range. By defining the point of fringe decorrelation as the point in time when the fringe visibility decreases by -3 dB, the upper timescale that should be used for this background subtraction scheme is roughly 40 seconds.

4. Experimental Procedure

The DHM was used to image two strains of bacteria (*Bacillus subtilis* and *Vibrio alginolyticus*), as well as the protozoan, *Euglena gracilis*. A 1 mm deep well was filled with a dilution of the biological sample in minimal media. A 'motility' medium was used for *B. subtilis* which would not harm the organisms but hinder their growth (10 mM phosphate buffer pH 7.4, 10 mM NaCl, 0.1 mM EDTA, 0.1 mM glucose). Due to the marine origins of *V. alginolyticus*, a different minimal media recipe was used (50 mM Tris buffer, 300 mM NaCl, 5 mM $MgCl_2$, 5 mM glucose). *E. gracilis* was diluted in spring water. Holographic images were recorded at a frame rate of 15 frames per second. Background image subtraction was performed with a timescale of 10 seconds (150 holograms). Both the raw holograms and background subtracted holograms were then spatially filtered and reconstructed via the angular spectrum method using either the commercial software KOALA (Lyncée Tec SA, www.lynceetec.com) or a Fiji-based plug-in developed by our group [3, 11, 12]. All bacterial

data were recorded using a monochromatic 405 nm laser illumination source. DHM images of *E. gracilis* were acquired using the multi-

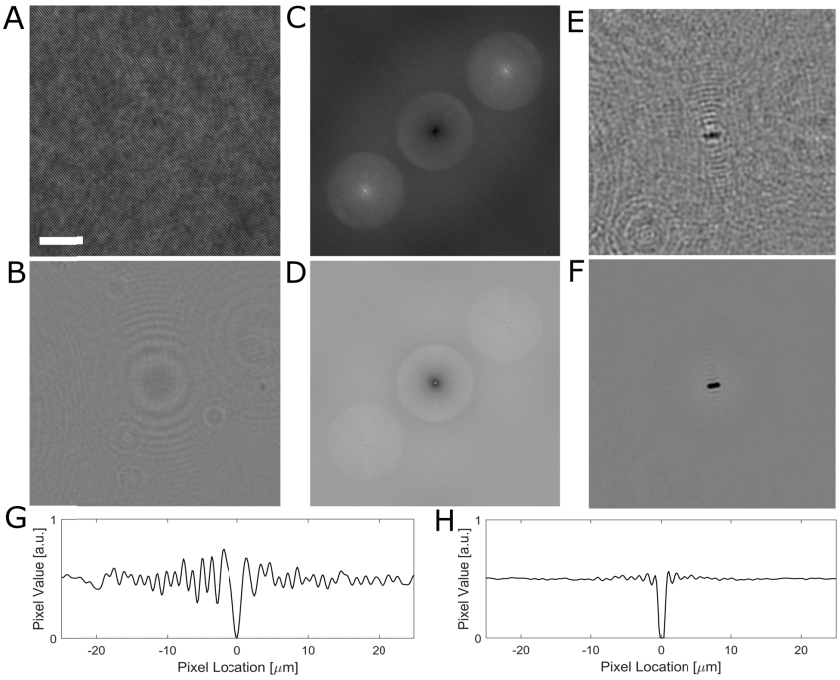

Fig. 2. Raw hologram of sample containing *B. subtilis* (A), the identical hologram after background subtraction (B), and their respective Fourier spectra (C and D). Intensity reconstruction of the same *B. subtilis* bacterium without (E) and with (F) the use of the residual fringe visibility analysis, as well as vertical line plots of pixel values through the bacterium (G and H, respectively). Scale bar represents 10 μm for (A, B, E, and F).

wavelength implementation of the common path DHM instrument, using a 405, 520, and 625 nm laser illumination source simultaneously.

5. Results

Figure 2 shows a raw hologram and background-subtracted hologram of a single *B. subtilis* bacterium (2A and 2B, respectively) and their respective Fourier spectra (2C and 2D). Figure 2E and 2F show the intensity reconstruction of the same bacterium using the raw hologram and background subtracted hologram, respectively, as well as vertical line plots of pixel values through the bacterium for both the raw reconstruction and background subtracted reconstruction (2G and 2H, respectively). Employing the background subtraction technique on data sets containing *B. subtilis* saw an increase in SNR of roughly an order of magnitude (11x improvement in SNR)

Figure 3 shows a raw and background subtracted hologram of a select *V. alginolyticus* bacterium (Figure 3A and 3B, respectively), and their respective Fourier spectra (Figure 3C and 3D). Figure 3E and 3F show a single plane intensity reconstruction of the same hologram from 3A and 3B, respectively. These intensity reconstructions also demonstrate an order of magnitude increase in SNR. Figure 3G and 3H show a volumetric rendering of intensity reconstructions using the raw and background subtracted holograms, respectively. These volumetric renderings have been thresholded to the same value for comparison. The implementation of the background subtraction technique can be seen to increase the SNR of volumetric intensity reconstructions to allow for the 3D localization of near diffraction limited objects such as *V. alginolyticus*. Due to the standard thresholding used in the volumetric renderings of 3G and 3H, vertical lines can be seen in Figure 3G, which are the

residual artifacts of the point spread function of the *V. alginolyticus*. Downstream processing techniques, such as deconvolution, would be effective in removing such artifacts.

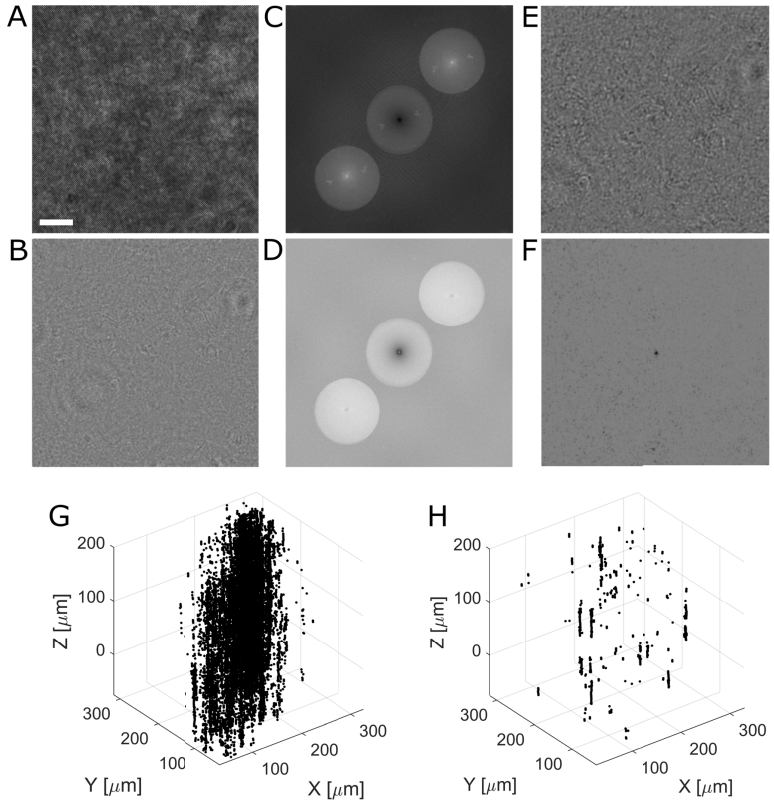

Fig. 3. Raw hologram of sample containing *V. alginolyticus* (A), the identical hologram after background subtraction (B), and their respective Fourier Spectra (C and D). Intensity reconstruction of the same *V. alginolyticus* bacterium without (E), and with (F) the use of the residual fringe visibility analysis, and a 3D rendering of the reconstructed intensity z-stack of the raw (G) and background subtracted hologram (H). Scale bar represents 10 μm for (A, B, E, and F).

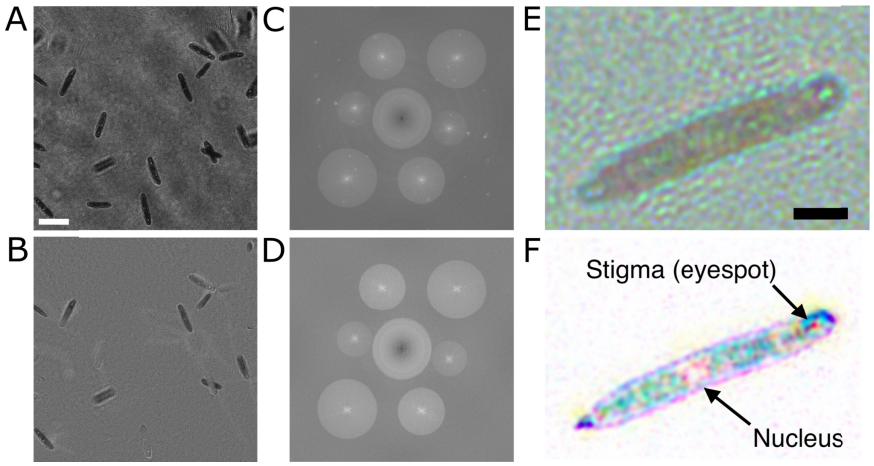

Fig. 4. Raw multiwavelength hologram of sample containing *E. gracilis* (A), the identical hologram after background subtraction (B), as well as their respective spectra (C and D,

respectively). A pseudo-colored composite intensity reconstruction of a select *E. gracilis* using the raw hologram (E), and background fringe subtraction technique (F). Scale bar in (A) represents 50 μm for both (A and B). Scale bar in (E) represents 20 μm for both (E and F).

Figure 4 shows a raw and background subtracted hologram of multi-wavelength DHM data containing *E. gracilis* (Figure 4A and 4B), and their respective Fourier spectra (Figure 4B and 4C). Figure 4D and 4E show a pseudo-colored composite intensity reconstructed image of a select *E. gracilis* using the raw and background subtracted hologram, respectively. The use of background subtracted holograms for multi-wavelegnth DHM data dramatically reduces the need for other post-processing unique to multi-wavelength data such as white balancing. Furthermore, the reduction in noise enables sub-cellular features of the *E. gracilis* to be much more visible, namely, the stigma (eyespot) and nucleus.

6. Conclusion

A novel method of enhancing image contrast of intensity reconstructions of digital off-axis holographic images is presented, including a theoretical justification, practical considerations in its implementation, and an experimental verification using biological samples. With roughly an order of magnitude of increased contrast provided by this method, standard image thresholding and clustering techniques become possible and enable high throughput and low computational overheard volumetric tracking. Furthermore, by conducting background subtraction on the raw holograms as opposed to the volumetric reconstruction, computational overhead is reduced proportionally to the number of axial planes reconstructed, potentially significantly decreasing computation times.

It is critical to note that fringe stability is necessary for this approach to work. We implemented it using a common-path off-axis DHM designed to be stable against vibrations. With a traditional Mach-Zehnder interferometer, the fringes may not be stable on the timescales reported in this work. Thus, the fringe stability and resultant number of frames used for background fringe subtraction will need to be determined for each instrument and light source combination.

Funding

This work was supported from the Jet Propulsion Laboratory (JPL), California Institute of Technology, under a contract with the National Aeronautics and Space Administration (NASA).

Disclosures

The authors declare no conflicts of interest.

References

1. Kim, M.K., L. Yu, and C.J. Mann, *Interference techniques in digital holography.* Journal of Optics A: Pure and Applied Optics, 2006. **8**(7): p. S518.
2. Bedrossian, M., et al. *Sources and propagation of errors in quantitative phase imaging techniques using optical interferometry*. in *Quantitative Phase Imaging III*. 2017. International Society for Optics and Photonics.
3. Cuche, E., P. Marquet, and C. Depeursinge, *Spatial filtering for zero-order and twin-image elimination in digital off-axis holography.* Applied Optics, 2000. **39**(23): p. 4070-4075.
4. Colomb, T., et al., *Total aberrations compensation in digital holographic microscopy with a reference conjugated hologram.* Optics express, 2006. **14**(10): p. 4300-4306.
5. De Nicola, S., et al., *Angular spectrum method with correction of anamorphism for numerical reconstruction of digital holograms on tilted planes.* Optics express, 2005. **13**(24): p. 9935-9940.
6. Grilli, S., et al., *Whole optical wavefields reconstruction by digital holography.* Optics Express, 2001. **9**(6): p. 294-302.
7. Stadelmaier, A. and J.H. Massig, *Compensation of lens aberrations in digital holography.* Optics letters, 2000. **25**(22): p. 1630-1632.
8. Wallace, J.K., et al., *Robust, compact implementation of an off-axis digital holographic microscope.* Optics Express, 2015. **23**(13): p. 17367-17378.

9. Lindensmith, C.A., et al., *A Submersible, Off-Axis Holographic Microscope for Detection of Microbial Motility and Morphology in Aqueous and Icy Environments.* PLOS ONE, 2016. **11**(1): p. e0147700.
10. Wallace, J.K., et al. *A multiwavelength digital holographic microscope architecture for enhancing life detection*. IEEE.
11. Cohoe, D., et al., *Multiwavelength digital holographic imaging and phase unwrapping of protozoa using custom Fiji plug-ins.* Frontiers in Physics, 2019. **7**: p. 94.
12. Schindelin, J., et al., *Fiji: an open-source platform for biological-image analysis.* Nature methods, 2012. **9**(7): p. 676-682.